the heart homogenates. For measurement of oxidized glutathione levels, samples were treated with 4-vinylpyridine (Wako, Osaka, Japan). Total glutathione and oxidized glutathione levels were determined by measuring the absorbance at 405nm of 5-thionitrobenzoic acid (TNB) and GS-TNB which derive from 5,5'-Dithiobis (2-nitrobenzoic acid) after reaction with glutathione. Glutathione levels in the heart were normalized to the weights of the myocardial tissues. Total glutathione to oxidized glutathione ratios were calculated as total glutathione levels divided by oxidized glutathione levels.

RNA Extraction and Real-Time PCR Analysis

Total RNA was isolated from the myocardial tissues and cultured cells with TRIzol Reagent (Invitrogen Corp., Carlsbad, CA, USA) and RNA Isolation Kit (Agilent Technologies, Santa Clara, CA, USA), respectively. Reverse transcription was performed with 1 μg of total RNA, random hexamer primers and MMLV reverse transcriptase (ReverTraAce-α; TOYOBO, Osaka, Japan). For quantitative assessment of gene expression levels, quantitative real time PCR analysis was performed. Specific mRNAs were quantified by SYBR Green real-time PCR Master Mix (TOYOBO, Osaka) in an ABI PRISM 7000 thermocycler (Applied Biosystems, Foster City, CA) under standard manufacturer's conditions. Data are expressed in arbitrary units that were normalized by correction for the signal obtained in the same cDNA preparation for GAPDH mRNA. The primers for real time PCR were shown in Supplemental Table Ⅱ.

Western Blot Analysis

Proteins were extracted from the myocardial tissues homogenized in a lysis buffer (PBS containing 1% Nonidet P-40, 0.1% SDS and 0.5% sodium deoxycholate) with a protease inhibitor cocktail (Sigma-Aldrich, St. Louis, MO, USA). Protein samples (30μg) were separated by SDS-PAGE and transferred to a polyvinylidene fluoride membrane (Hybond-P; GE Healthcare, Little Chalfont, UK). The membrane was incubated with anti-ABCG2 antibody (1:100; BXP-53; Alexis Biochemicals, Farmingdale, NY, USA) and anti-β-actin antibody (1:5000; AC-15; Sigma-Aldrich, St. Louis, MO, USA), followed by incubation with horseradish peroxidase-conjugated secondary antibody. The enhanced chemiluminescence system (ECL Plus; GE Healthcare, Little Chalfont, UK) was used for detection. The densitometric values of bands were measured using the densitometry software (Multi Gauge Ver3.0, FUJIFILM, Tokyo, Japan). Signal intensity was normalized to β-actin expression.

Cell Cultures

Human microvascular endothelial cells from the heart (HMVEC-Cs) were purchased from Lonza (Basel, Switzerland). HMVEC-Cs were cultured in EGM-2 medium (Lonza, Basel, Switzerland) at 37℃ in a mixture of 95% air and 5% CO_2. *Abcg2* knockdown in HMVEC-Cs was performed by using ABCG2 siRNA (Santa Cruz Biotechnology, Santa Cruz, CA, USA) according to the manufacturer's protocol. Control siRNA (Santa Cruz Biotechnology, Santa Cruz, CA, USA) was also transfected into HMVEC-Cs as a control experiment.

Cardiomyocytes were prepared from neonatal rats and cultured as described previously with minor modifications.[8] Neonatal Wistar rats were purchased from Takasugi Experimental Animal

Supply (Saitama, Japan). Neonatal ventricles from 1-day-old Wistar rats were separated and minced in ice-cold balanced salt solution. For isolation of cardiac cells, the tissues were incubated in a balanced salt solution containing 0.2% collagenase type 2 (Worthington Biochemical, Lakewood, NJ, USA) for 7 minutes at 37℃ with agitation. The digestion buffer was replaced 7 times. The dispersed cells were incubated in 100-mm culture dishes for 90 minutes to remove non-myocytes. The unattached viable cells, which were rich in cardiomyocytes, were cultured on collagen type Ⅰ-coated dishes at 37℃ in DMEM supplemented with 10% fetal bovine serum (FBS).

Measurement of Extracellular and Intracellular Glutathione Concentrations in HMVEC-Cs

Extracellular and intracellular glutathione concentration in HMVEC-Cs was measured using Total glutathione assay kit (Northwest Life Science Specialities LLC, Vancouver, WA, USA) according to the manufacturer's guidelines. Briefly, HMVEC-Cs were cultured in 24 well dish at 80% confluency, and were exposed to vehicle or 2',5'-dihydroxychalcone (2',5'-DHC, 25μmol/L, INDOFINE Chemical Company, Inc., Hillsborough, NJ, USA) for 24 hours with presence or absence of 10 μmol/L fumitremorgin C (FTC), a specific inhibitor of ABCG2 (n=4 for each group). Cell lysate protein values were measured using BCA protein assay kit (Pierce Biotechnology, Rockford, IL, USA), and were used to normalize glutathione values. Deproteination was performed using 5% metaphosphoric acid added to both media and cell lysates. Glutathione concentrations were determined by measuring the absorbance at 405nm of 5-thionitrobenzoic acid (TNB) and GS-TNB which derive from 5,5'-Dithiobis after reaction with glutathione. Extracellular and intracellular glutathione concentration

in HMVEC-Cs treated with siRNA was also measured after 24-hour exposure to vehicle or 2',5'-DHC.

Production of Medium Conditioned by HMVEC-Cs

HMVEC-Cs were cultured in 100-mm dishes at 80% confluency. The medium was then replaced with fresh EBM-2 medium (Lonza, Basel, Switzerland) supplemented with 10% FBS and 1% penicillin-streptomycin, and the cells were exposed to vehicle or 25μmol/L 2',5'-DHC for 24 hours with presence or absence of 10 μmol/L FTC. The medium was then collected as conditioned medium.

Cardiomyocyte Culture in HMVEC-C-Conditioned Medium

Isolated cardiomyocytes were cultured in DMEM supplemented with 10% FBS for 24 hours, after which the culture medium was replaced with medium conditioned by HMVEC-Cs. Cardiomyocytes were then exposed to vehicle or 30μmol/L hydrogen peroxide for 48 hours.[9] After 48 hour incubation, the cells were fixed in 2% paraformaldehyde and permeabilized for 10 minutes with 0.2% Triton-X (Sigma-Aldrich, St. Louis, MO, USA) in PBS. After blocking with PBS containing 2% FBS for 10 minutes, they were then incubated with anti-sarcomeric α-actinin antibody (Sigma-Aldrich, St. Louis, MO, USA), followed by treatment with an Alexa Fluor 488-conjugated secondary antibody. Cardiomyocyte size was determined by measuring the cell surface areas of sarcomeric α-actinin-positive cells.

Statistical Analysis

Data are shown as mean±SEM. Kaplan-Meier method and the log-rank test were used for comparison of survival. Differences in means between 2 groups were analyzed by unpaired Student's t-test.

Multiple group comparison was performed by one-way analysis of variance (ANOVA) followed by Student-Newman-Keuls post hoc test. When the number of samples was different among groups, Scheffe's test was used as the post hoc test. Values of $P<0.05$ were considered statistically significant.

Supplemental References

1. Institute of Laboratory Animal Resources (U.S.). Committee on Care and Use of Laboratory Animals., National Institutes of Health (U.S.). *Guide for the care and use of laboratory animals*. Rev. 1985.ed. [Bethesda, Md.]: U.S. Dept. of Health and Human Services, Public Health Service, National Institutes of Health; 1985.

2. Jonker JW, Buitelaar M, Wagenaar E, Van Der Valk MA, Scheffer GL, Scheper RJ, Plosch T, Kuipers F, Elferink RP, Rosing H, Beijnen JH, Schinkel AH. The breast cancer resistance protein protects against a major chlorophyll-derived dietary phototoxin and protoporphyria. *Proc Natl Acad Sci U S A.* 2002;99:15649-15654.

3. Rockman HA, Ross RS, Harris AN, Knowlton KU, Steinhelper ME, Field LJ, Ross J, Jr., Chien KR. Segregation of atrial-specific and inducible expression of an atrial natriuretic factor transgene in an in vivo murine model of cardiac hypertrophy. *Proc Natl Acad Sci U S A.* 1991;88:8277-8281.

4. D'Apolito M, Du X, Zong H, Catucci A, Maiuri L, Trivisano T, Pettoello-Mantovani M, Campanozzi A, Raia V, Pessin JE, Brownlee M, Giardino I. Urea-induced ROS generation causes insulin resistance in mice with chronic renal failure. *J Clin Invest*. 2010;120:203-213.

5. Sumi M, Sata M, Miura S, Rye KA, Toya N, Kanaoka Y, Yanaga K, Ohki T, Saku K, Nagai R. Reconstituted high-density lipoprotein stimulates differentiation of endothelial progenitor cells and enhances ischemia-induced angiogenesis. *Arterioscler Thromb Vasc Biol.*

2007;27:813-818.

6. Nakamura K, Sata M, Iwata H, Sakai Y, Hirata Y, Kugiyama K, Nagai R. A synthetic small molecule, ONO-1301, enhances endogenous growth factor expression and augments angiogenesis in the ischaemic heart. *Clin Sci (Lond).* 2007;112:607-616.

7. Higashikuni Y, Sainz J, Nakamura K, Takaoka M, Enomoto S, Iwata H, Sahara M, Tanaka K, Koibuchi N, Ito S, Kusuhara H, Sugiyama Y, Hirata Y, Nagai R, Sata M. The ATP-binding cassette transporter BCRP1/ABCG2 plays a pivotal role in cardiac repair after myocardial infarction via modulation of microvascular endothelial cell survival and function. *Arterioscler Thromb Vasc Biol.* 2010;30:2128-2135.

8. Takeda N, Manabe I, Uchino Y, Eguchi K, Matsumoto S, Nishimura S, Shindo T, Sano M, Otsu K, Snider P, Conway SJ, Nagai R. Cardiac fibroblasts are essential for the adaptive response of the murine heart to pressure overload. *J Clin Invest.* 2010;120:254-265.

9. Kwon SH, Pimentel DR, Remondino A, Sawyer DB, Colucci WS. H(2)O(2) regulates cardiac myocyte phenotype via concentration-dependent activation of distinct kinase pathways. *J Mol Cell Cardiol.* 2003;35:615-621.

Supplemental Figure Legends

Supplemental Figure Ⅰ. ABCG2 expression levels in the heart after TAC. (A) ABCG2 mRNA expression in the heart after TAC (n=4 for each group). B, baseline. *P<0.05 versus baseline; †P<0.05 versus sham. (B) ABCG2 protein expression in the heart after TAC (n=3 for each group). Western blot analysis was performed. *P<0.05 versus baseline.

Supplemental Figure Ⅱ. Autopsy of dead *Abcg2*$^{-/-}$ mice at 4 days after TAC. (A-C) Heart weight (HW) to body weight (BW) ratios (A), cross-sectional area (CSA) of cardiomyocytes (B) and collagen volume fraction (CVF) (C) in dead *Abcg2*$^{-/-}$ mice at 4 days after TAC were assessed and compared with those in sham-operated *Abcg2*$^{-/-}$ mice (n=3 for each group). Cardiac hypertrophy and interstitial fibrosis were found in dead *Abcg2*$^{-/-}$ mice at 4 days after TAC. S, sham-operated mice; D, dead mice. *P<0.05 versus sham. (D) Representative images of the lungs. Note pulmonary congestion in dead *Abcg2*$^{-/-}$ mice at 4 days after TAC. (E) Lung weight was assessed in dead *Abcg2*$^{-/-}$ mice at 4 days after TAC. *P<0.05 versus sham.

Supplemental Figure Ⅲ. Cardiomyocyte hypertrophy and cardiac fibrosis after TAC. (A) Cross-sectional area (CSA) of cardiomyocytes was measured in specimens with H&E staining (n=5 for each group). Scale bars=20 μm. (B) Collagen volume fraction (CVF) was measured in specimens with sirius red staining (n=5 for each group). Scale bars=50 μm. (C) Hypertrophic marker gene

expression. Expression of ANF and BNP was quantified by real-time PCR (n=4 for each group). (D) Fibrosis-related gene expression. Expression of collagen type 1 alpha 1 (COL1A1), collagen type 3 alpha 1 (COL3A1), TGF-β1 and fibronectin was quantified by real-time PCR (n=4 for each group). Open columns, wild-type (WT) mice; filled columns, *Abcg2*$^{-/-}$ (KO) mice. B, baseline; D4, 4 days after TAC; D28, 28 days after TAC. *P<0.05 versus WT mice at baseline; †P<0.05 versus KO mice at baseline; ‡P<0.05 versus WT mice at the same post-operative day.

Supplemental Figure Ⅳ. ABCG2 expression and angiogenesis after hindlimb ischemia. (A) Representative images of immunohistochemistry with anti-ABCG2 staining. ABCG2 is abundantly expressed in the kidney and the liver. Scale bars indicate 50 μm for the kidney and 20 μm for the liver. (B) Angiogenesis after hindlimb ischemia. Unilateral hindlimb ischemia was induced in 14– to 17–week old WT and *Abcg2*$^{-/-}$ mice (n=10 for WT mice; n=12 for *Abcg2*$^{-/-}$ mice). Hindlimb perfusion was measured with a laser Doppler imaging system. The blood flow of the ischemic hindlimb was expressed as the ratio to that of the uninjured limb. No significant differences were found between wild-type (WT) and *Abcg2*$^{-/-}$ (KO) mice. W, week after the operation.

Supplemental Figure Ⅴ. Expression levels of the tumor suppressor p53 after TAC. Expression of p53 was quantified by real-time PCR (n=4 for each group). Open columns, wild-type (WT) mice; filled columns, *Abcg2*$^{-/-}$ (KO) mice. B, baseline; D4, 4 days after TAC; D28, 28 days after TAC.

*P<0.05 versus WT mice at baseline; †P<0.05 versus KO mice at baseline; ‡P<0.05 versus WT mice at the same post-operative day.

Supplemental Figure Ⅵ. Inflammatory response in the heart after TAC. (A) Pro-inflammatory cytokine expression. Expression levels of TNF-α, IL-6 and MCP-1 were assessed by real-time PCR (n=4 for each group). (B) Macrophage density in the heart after TAC (n=5 for each group). Scale bars=20 μm. Open columns, wild-type (WT) mice; filled columns, *Abcg2*$^{-/-}$ (KO) mice. B, baseline; D4, 4 days after TAC; D28, 28 days after TAC. *P<0.05 versus WT mice at baseline; †P<0.05 versus KO mice at baseline; ‡P<0.05 versus WT mice at the same post-operative day.

Supplemental Figure Ⅶ. Total glutathione (GSH) to oxidized glutathione (GSSG) ratios in plasma and the heart after TAC. Open columns, wild-type (WT) mice; filled columns, *Abcg2*$^{-/-}$ (KO) mice. B, baseline. *P<0.05 versus WT mice at baseline; †P<0.05 versus KO mice at baseline; ‡P<0.05 versus WT mice at the same post-operative day.

Supplemental Figure Ⅷ. Echocardiographic data at 4 days after TAC under PBS or MnTBAP treatment (n=5 for each group). Open columns, wild-type (WT) mice; filled columns, *Abcg2*$^{-/-}$ (KO) mice. LVEDD, left ventricle end-diastolic diameter; EF, ejection fraction; IVSth, interventricular septum thickness; LVPWth, left ventricle posterior wall thickness; W, WT mice; K, KO mice; P, PBS

group; M, MnTBAP group. *P<0.05 versus sham; †P<0.05 versus WT mice with the same treatment; ‡P<0.05 versus PBS group after the same operation.

Supplemental Figure Ⅸ. Hemodynamic data at 28 days after TAC under PBS or MnTBAP treatment (n=3 for each group). Open columns, wild-type (WT) mice; filled columns, *Abcg2*$^{-/-}$ (KO) mice. LVEDP, left ventricular end-diastolic pressure; W, WT mice; K, KO mice; P, PBS group; M, MnTBAP group. *P<0.05 versus sham; †P<0.05 versus WT mice with the same treatment; ‡P<0.05 versus PBS group after the same operation.

Supplemental Figure Ⅹ. Cardiomyocyte hypertrophy and cardiac fibrosis at 28 days after TAC under PBS or MnTBAP treatment. (A) Representative images of H&E staining. Scale bars=20 μm. (B) Representative images of sirius red staining. Scale bars=50 μm. WT, wild-type mice; KO, *Abcg2*$^{-/-}$ mice.

Supplemental Figure Ⅺ. Angiogenesis in the heart at 28 days after TAC under PBS or MnTBAP treatment. Representative images of anti-CD31 staining. Scale bars=20 μm. WT, wild-type mice; KO, *Abcg2*$^{-/-}$ mice.

Supplemental Figure Ⅻ. Macrophage density at 28 days after TAC under PBS or MnTBAP

treatment (n=3 for sham; n=4 for TAC). Scale bars=20 μm. Open columns, wild-type (WT) mice; filled columns, *Abcg2*$^{-/-}$ (KO) mice. W, WT mice; K, KO mice; P, PBS group; M, MnTBAP group. *P<0.05 versus sham; †P<0.05 versus PBS group after the same operation.

Supplemental Table Ⅰ. Echocardiographic, Hemodynamic and Histological Data on Sham-Operated Mice.

	WT		KO	
	Baseline	Day 28	Baseline	Day 28
Echocardiography				
n	11	11	11	11
LVEDD, mm	3.555±0.008	3.559±0.006	3.539±0.010	3.545±0.005
EF, %	65.7±0.5	67.0±0.6	67.0±0.7	66.1±0.3
IVSth, mm	0.715±0.002	0.713±0.002	0.718±0.001	0.714±0.002
LVPWth, mm	0.726±0.002	0.727±0.002	0.725±0.003	0.723±0.002
Hemodynamic data				
n	-	5	-	5
LVEDP, mmHg	-	1.76±0.16	-	1.81±0.12
+dp/dt maximum, mmHg/s	-	8210±283	-	8145±630
-dp/dt minimum, mmHg/s	-	-5266±345	-	-5856±351
Systolic BP, mmHg	-	81.5±2.9	-	82.2±2.2
Histological data				
n		5		5
Myocyte CSA, μm^2	-	170.0±2.6	-	170.2±2.1
CVF, %	-	0.44±0.03	-	0.39±0.05
HW to BW ratio, mg/g	-	6.11±0.15 (n=11)	-	6.15±0.08 (n=11)

WT, wild-type mice; KO, *Abcg2*$^{-/-}$ mice; LVEDD, left ventricle end-diastolic diameter; EF, ejection fraction; IVSth, interventricular septum thickness; LVPWth, left ventricle posterior wall thickness; LVEDP, left ventricular end-diastolic pressure; BP, blood pressure; CSA, cross-sectional area; CVF, collagen volume fraction; HW, heart weight; BW, body weight.

Supplemental Table Ⅱ. Sequence of Primers for Real-Time PCR

Primer	Forward	Reverse	Product length
Mouse			
ABCG2	GCCTTGGAGTACTTTGCATCA	AAATCCGCAGGGTTGTTGTA	63
ANF	GGGTAGGATTGACAGGATTGGA	CGACTGCCTTTTCCTCCTTG	91
BNP	AGGCGAGACAAGGGAGAACA	GGTGACAGATAAAGGAAAAGCAGAA	115
TGF-β1	GCCTGAGTGGCTGTCTTTTG	CGTGGAGTTTGTTATCTTTGCTGT	125
Fibronectin	TGTGAAAGGGAACCAGCAGA	CTCGGTGTTGTAAGGTGGAATG	88
COL1A1	CCGAACCCCAAGGAAAAGA	GTGGACATTAGGCGCAGGA	134
COL3A1	TCCCCTGGAATCTGTGAATC	TGAGTCGAATTGGGGAGAAT	63
HIF-1α	CCCATTCCTCATCCGTCAA	CCGGCTCATAACCCATCAA	127
HIF-2α	CAGGTAGAACTAACAGGACACAGCA	AGAAGTCACGCTCGGTGGA	139
VEGFA	AAAAACGAAAGCGCAAGAAA	TTTCTCCGCTCTGAACAAGG	73
Angiopoietin-1	CGGATTTCTCTTCCCAGAAAC	TCCGACTTCATATTTTCCACAA	107
NOX2	GAGGTTGGTTCGGTTTTGG	GTTTTGAAAGGGTGGGTGAC	72
NOX4	CAGTCCTGGCTTATCTTCGAG	GAGTCTTGCTTTTATCCAACAATCT	78
XO	GGAGATATTGGTGTCCATTGTG	CCTGCTTGAAGGCTGAGAAA	68
NOS3	AGCGTGTGAAGGCAACCA	GGACACCACATCATACTCATCCA	134
Nrf2	ATGATGGACTTGGAGTTGCC	TCCTGTTCCTTCTGGAGTTG	200
SOD1	CAGGACCTCATTTTAATCCTCAC	TGCCCAGGTCTCCAACAT	78
SOD2	TCCCAGACCTGCCTTACGA	TCGGTGGCGTTGAGATTG	115
SOD3	GGGGAGGCAACTCAGAGG	TGGCTGAGGTTCTCTGCAC	112
γ-GCS	GCACATCTACCACGCAGTCAA	CATCGCCTCCATTCAGTAACAA	128
GPx1	TTTCCCGTGCAATCAGTTC	TCGGACGTACTTGAGGGAAT	76
Catalase	CCTTCAAGTTGGTTAATGCAGA	CAAGTTTTTGATGCCCTGGT	80
Thioredoxin 1	TGAAGCTGATCGAGAGCAAG	AGAAGTCCACCACGACAAGC	78
Thioredoxin 2	CACACAGACCTTGCCATTGA	CACGTCCCCGTTCTTGAT	72
TNF-α	TCCCAGGTTCTCTTCAAGGGA	GGTGAGGAGCACGTAGTCGG	51
IL-6	ACAACCACGGCCTTCCCTACTT	CACGATTTCCCAGAGAACATGTG	129
MCP-1	CCACTCACCTGCTGCTACTCAT	TGGTGATCCTCTTGTAGCTCTCC	76
p53	CCGACCTATCCTTACCATCATCAC	GGCACAAACACGAACCTCAA	85
GAPDH	ATGACAACTTTGTCAAGCTCATTT	GGTCCACCACCCTGTTGCT	69
Human			
ABCG2	AACTGAAGAGTGGCTTTCTACCTTG	ATAACGAAGATTTGCCTCCACCT	129
GAPDH	CGCTCTCTGCTCCTCCTGTT	AAATCCGTTGACTCCGACCTT	110

NOX, NADPH oxidase; XO, xanthine oxidase; NOS, nitric oxide synthase; SOD, superoxide dismutase; γ -GCS, γ-glutamylcysteine synthase; GPx, glutathione peroxidase.

Supplemental Figure I

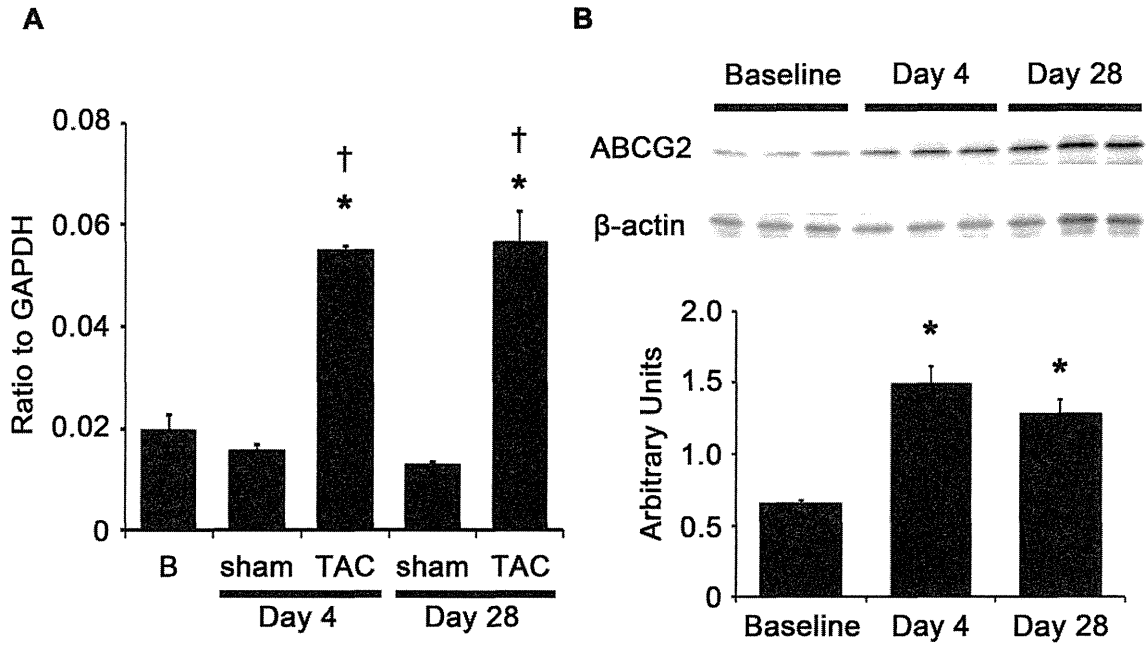

Supplemental Figure Ⅱ

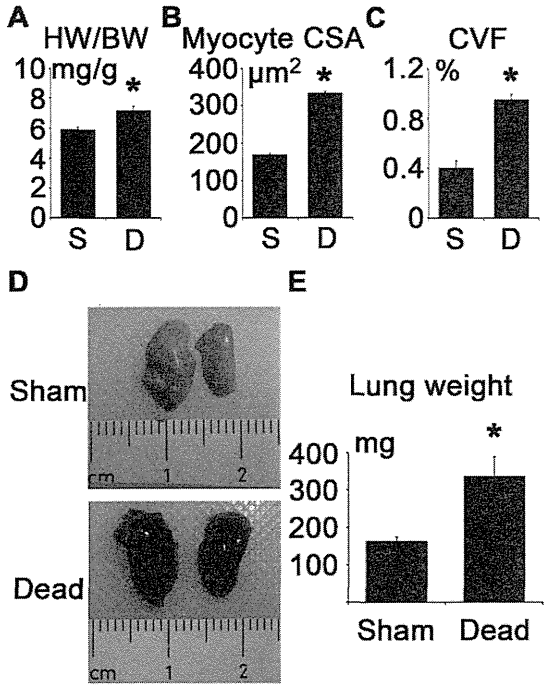

Supplemental Figure Ⅲ

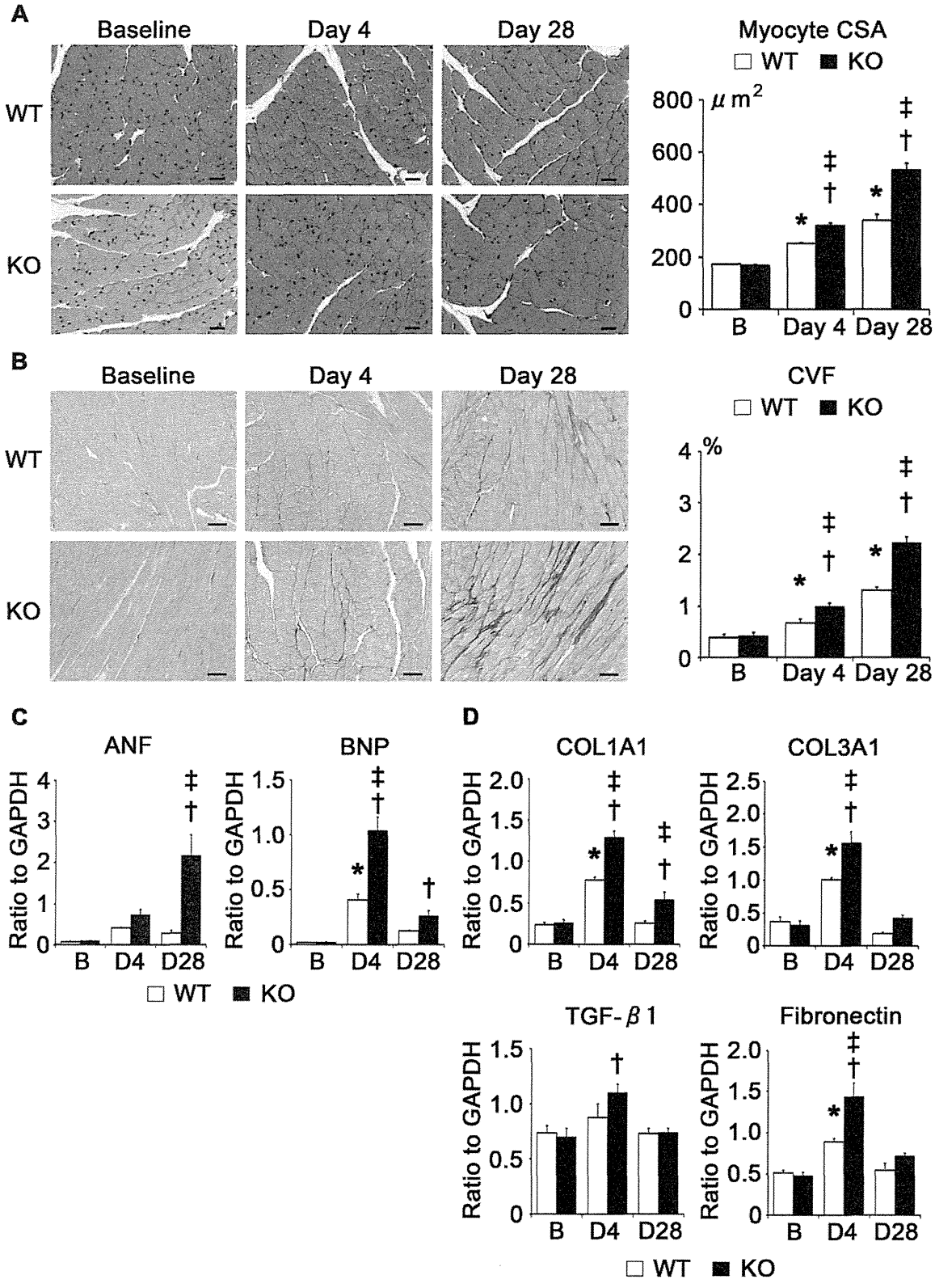

Supplemental Figure Ⅳ

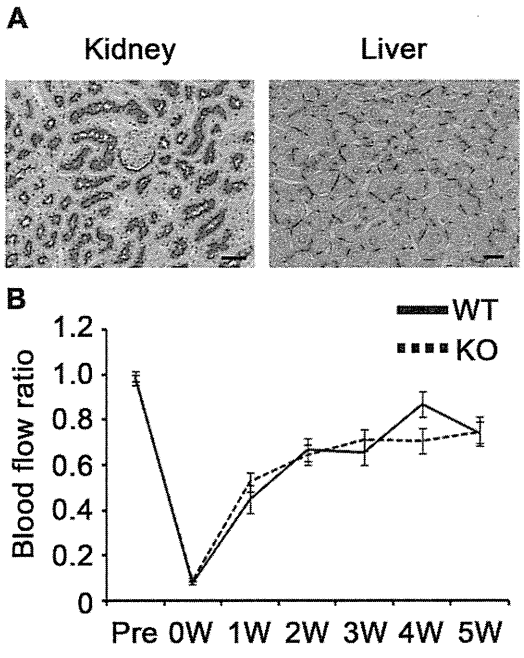

Supplemental Figure V

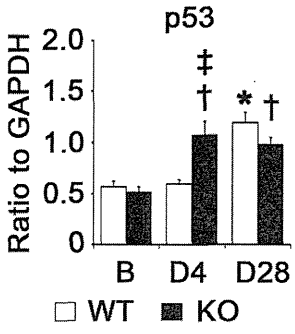

Supplemental Figure VI